Chinese Journal of Aeronautics, (2018), 31(5): 1041–1052

Chinese Society of Aeronautics and Astronautics
& Beihang University

Chinese Journal of Aeronautics

cja@buaa.edu.cn
www.sciencedirect.com

Nonlinear dynamics of a flapping rotary wing: Modeling and optimal wing kinematic analysis

Qiuqiu WEN [a,*], **Shijun GUO** [b], **Hao LI** [b], **Wei DONG** [a]

[a] *School of Aerospace, Beijing Institute of Technology, Beijing 100081, China*
[b] *Centre for Aeronautics, SATM, Cranfield University, Cranfield MK43 0AL, UK*

Received 17 April 2017; revised 15 May 2017; accepted 21 August 2017
Available online 13 March 2018

KEYWORDS

Dynamic model;
Dynamic time-lag;
Flapping rotary wing;
Kinematics of wings;
Passive rotation;
Strike angle

Abstract The analysis of the passive rotation feature of a micro Flapping Rotary Wing (FRW) applicable for Micro Air Vehicle (MAV) design is presented in this paper. The dynamics of the wing and its influence on aerodynamic performance of FRW is studied at low Reynolds number ($\sim 10^3$). The FRW is modeled as a simplified system of three rigid bodies: a rotary base with two flapping wings. The multibody dynamic theory is employed to derive the motion equations for FRW. A quasi-steady aerodynamic model is utilized for the calculation of the aerodynamic forces and moments. The dynamic motion process and the effects of the kinematics of wings on the dynamic rotational equilibrium of FWR and the aerodynamic performances are studied. The results show that the passive rotation motion of the wings is a continuous dynamic process which converges into an equilibrium rotary velocity due to the interaction between aerodynamic thrust, drag force and wing inertia. This causes a unique dynamic time-lag phenomena of lift generation for FRW, unlike the normal flapping wing flight vehicle driven by its own motor to actively rotate its wings. The analysis also shows that in order to acquire a high positive lift generation with high power efficiency and small dynamic time-lag, a relative high mid-up stroke angle within 7–15° and low mid-down stroke angle within −40° to −35° are necessary. The results provide a quantified guidance for design option of FRW together with the optimal kinematics of motion according to flight performance requirement.

1. Introduction

The Micro Air Vehicle (MAV) has become an active research area due to the potentiality for the civil and military application.[1] The typical characteristics of MAV are small dimension (wing spans within 15 cm), low weight (gross take-off weight ranging from 100 to 200 g) and low flight speed (between 10 and 15 m/s). In recent two decades, a variety of MAV layouts, which mainly include fixed wing, rotary wing, and flapping wing, had been put forward. However, due to the extremely small dimension and high lift and efficiency requirements at

* Corresponding author.
E-mail address: wenqiuqiu82@bit.edu.cn (Q. WEN).
Peer review under responsibility of Editorial Committee of CJA.

https://doi.org/10.1016/j.cja.2018.03.004
1000-9361

Nomenclature

C_H, C_V	translational force coefficient along x_w axis and y_w axis
C_L, C_D	lift and drag coefficients
$\bar{C}_{L\_stab}$	period average lift coefficient
C_r	rotational force coefficient
$\boldsymbol{C}_t$	translational force coefficients
c	chord length of the wing
$\bar{c}$	mean chord length of the wing
$d\boldsymbol{M}_q$	aerodynamic torque of the above two forces
$d\boldsymbol{F}_a$	virtual mass force
$d\boldsymbol{M}_a$	virtual mass moment
$\boldsymbol{e}_{x,w}$, $\boldsymbol{e}_{y,w}$, $\boldsymbol{e}_{z,w}$	unit vectors of right wing frame
$\boldsymbol{F}_{aero}$, $\boldsymbol{M}_{aero}$	total aerodynamic forces and moments
$\boldsymbol{F}_i^*$	inertia force of the ith rigid body
$\boldsymbol{F}_t$, $\boldsymbol{F}_r$	translational and rotational forces
f_F	flapping frequency
$\boldsymbol{I}_i$	resulting mass moments of inertia matrices for each rigid body
i_{stab}	flapping period while FRW has been in the ERS
$\boldsymbol{M}_i^*$	inertia moment of the ith rigid body
$\boldsymbol{M}_{mass}$	gravity moments due to the mass of wings
$\boldsymbol{M}_w$	aerodynamic moments produced by flapping wings
m_i	mass of the ith rigid body
$O_b x_b y_b z_b$	body frame
$O_r x_r y_r z_r$	rotary plane frame
$O_w x_w y_w z_w$	wing-fixed frames
$\bar{P}_f$	average power output
$\bar{P}_{f\_stab}$	power efficiency coefficient
Q_j^*	functions of generalized inertia force
R	span length of wing
$\boldsymbol{R}_{br}$	rotation matrix from the body frame to rotation plane frame
$\boldsymbol{R}_{bwR}$, $\boldsymbol{R}_{bwL}$	rotation matrix from the body frame to right wing and left frames
$\boldsymbol{R}_{Ib}$	transfer matrix from inertial frame to body frame
r_{CP}	location of the Centre of Pressure (CP) at a chord-wise location
S_w	the size of wing
T_F	flapping period
$\bar{t}$	time courses of wing motion during a flapping period
t_0	initial time at the beginning of one flapping period
$\boldsymbol{u}_i$	related quasi-velocities of coordinates
$\boldsymbol{v}_i$	velocities of the ith rigid body
$\boldsymbol{v}_w(r)$	velocity of a chord-wise location on the wing
v_t	flapping velocity at the wingtip
x_b, y_b, z_b	axes of the body frame
x_i	generalized coordinates of the five degrees of freedom
α_e	effective angle of attack of the wing
α_U, α_D	mid up-stroke and down-stroke angles
$\boldsymbol{\beta}_{ij}$	angular velocity coefficients
$\boldsymbol{\gamma}_{ij}$	velocity coefficients
$\Delta\gamma_w$	flapping amplitude angle
$\Delta\alpha$	pitching amplitude
ϑ_w, γ_w	pitch angle and flap angle
λ_a, $\lambda_{a\omega}$	added mass force coefficients
$\bar{\mu}_{f\_stab}$	nondimensional rotational velocity
ρ	density of the surrounding air
$\boldsymbol{\rho}_i$	reference vectors of the ith rigid body
ψ_{j0}	rotating speed
ψ_r	rotation angle of rotary base
$\boldsymbol{\omega}_i$	angular velocities of the ith rigid body

Subscripts

b	the body of FRW
i	the number of rigid bodies
j	the number of generalized coordinates
wL, wR	the left and right wing

low Reynolds numbers Re, few practical MAVs with load carrying capabilities has been accomplished. Research efforts for new and practical designs of MAVs have never been stopped.

In 2004, Vandenberghe et al.[2] employed the experimental method and found that a pair of wing flapping up and down can freely rotate spontaneously around the horizontal shaft as a critical frequency was exceeded. Based on this discovery, Guo et al.[3,4] proposed the design of Flapping Rotary Wing (FRW) flight vehicle as a new configuration of MAV. Similar concept was also proposed and applied in full-scaled helicopter rotor by Van Holten et al.[5] As shown in Fig. 1, a pair of anti-symmetrically mounted wings, which can flap along the vertical direction by a drive shaft, is fixed on the rotary rigid base. The thrust generated by the wings' vertically flapping motion drives them to rotate around the shaft, resulting in a flapping and simultaneously rotating kinematics. Combined with tuning the pitch angles of the wings asymmetrically in the up-stroke and down-stroke, the high lift force is produced to make FRW take-off and hover.

Recently, experimental works[6] were used to measure the force produced and proved that the lift from flapping rotary wing was larger than that from conventional rotary wing in the range of Re from 2600 to 5000. Wu et al.[7] conducted a computational fluid dynamics method to research the unsteady aerodynamic behavior of FRW. It is observed that the leading-edge vortex attached on the wing surface during the whole flapping period, which is the main reason for the high lift generation by FRW. Unlike the ordinary Flapping Wing (FW) flight vehicle which is driven by its own motor to rotate, the flapping rotary wing is driven by the aerodynamic force to rotate passively. Previous works on FRW have mostly assigned a constant rotation velocity by assuming an 'equilibrium' state. However, for a practical wing, the inertia forces associated with the complicated kinematics will essentially interact with the aerodynamic force production. The influence of the wing inertia and the dynamic process as the wing converges to the equilibrium status will necessarily have a nontrivial effect on the aerodynamic performance of FRW. The

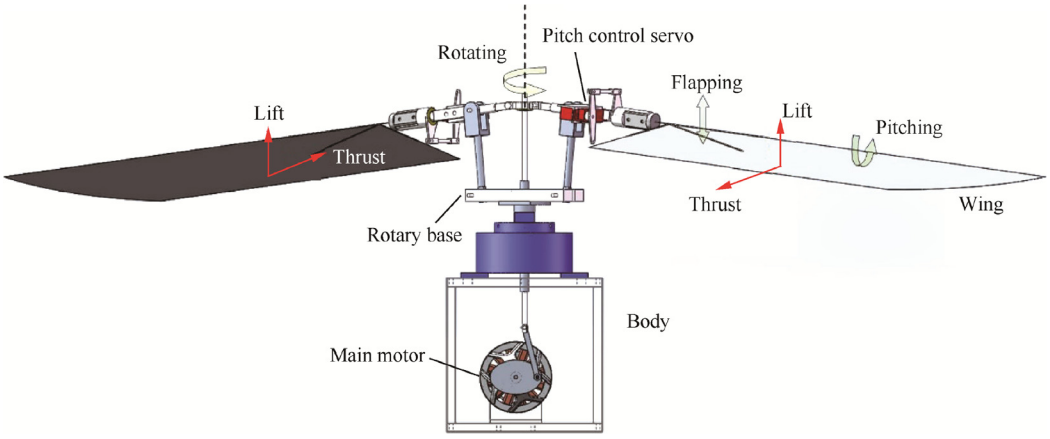

Fig. 1 Configuration of FRW flight vehicle.

varying rotation velocity conversely affects the aerodynamics and flow structure of the flapping rotary wing,[8] resulting in a coupling between the passively rotary motion and aerodynamic force. Therefore, the nonlinear dynamic model, especially for FRW, is needed to analyze its aerodynamic performance.

To date, only a few studies have focused on the dynamics of FRW. However, many studies have been relevant to flapping wing flight vehicle. In these studies, dynamics of FW are generally investigated using standard aircraft equations with six degrees of freedom.[9,10] However, this approach neglects the inertial effects of the mass of the wings. Recently, some studies have investigated the dynamics from the aspect of multiple-body nonlinear system, such as Gebert[11] and Sun[12] et al. Orlowski and Girard[13] modeled a flapping wing micro air vehicle as a system of three rigid bodies, a body and two wings, and studied the influence of the mass of the wings to the dynamics. Mahjoubi and Byl[14] developed the dynamic multi-body model using Lagrangian method and the proposed control approach to optimize the wings' mass and mechanical impedance properties of the joints. These studies have indicated that the multiple-body dynamic theory may be used to analyze the dynamics of FRW.

In this paper, a simplified FRW is modeled as three rigid bodies, one for the body of rotary base and others for each wing. The wing pitching motion is assumed to be actively driven through a control servo, as shown in Fig. 1. Thereby, each flapping wing owns three degrees of freedom: the actively flapping, pitching and the passively rotating. Using the D' Alembert's Principle given in Ref.[15], a multi-body dynamic model is derived for FRW. In addition, a quasi-steady aerodynamic model is utilized for the calculation of the aerodynamic forces and moments. The motion process of wings is simulated in a selected typical parameter set to understand the coupling with the lift/thrust production. Finally, the effects of the kinematics of wings on the dynamic rotational equilibrium of FWR and the aerodynamic performances are presented.

2. Reference definition

To describe the motion of rotary base in the FWR body frame, and the motion of wings with respect to rotary base, four reference frames are used. The body frame $O_b x_b y_b z_b$ is attached to the center of the body of FWR. As shown in Fig. 2, the positive x_b axis is along the longitudinal axis of the central body. The y_b axis locus in the vertical symmetry plane of body and is perpendicular to the x_b axis with a positive upward. The z_b axis is perpendicular to the xOy plane. The unit vectors of the body frame are presented by $\boldsymbol{e}_{x,b}$, $\boldsymbol{e}_{y,b}$ and $\boldsymbol{e}_{z,b}$.

After rotating an angle ψ_r about the y_b axis of the body frame for the rotary base, it becomes the rotary plane frame $O_r x_r y_r z_r$ (shown as the subscript "r"). The rotate plane frame defines the rotary motion of two connected wings.

The wing-fixed frames $O_w x_w y_w z_w$ are two fixed frames attached to the wings. The initial orientation of the wing-fixed frames is parallel to the rotate plane frame with an origin coincident with the rotation of the wings joint. The orientation of the wings with respect to the rotary plane is determined by the pitch angle ϑ_w and flap angle γ_w of the wings. Here we use the subscripts L, R to represent the left and right wings, respectively.

The rotation matrix from the body frame to rotation plane frame is

$$\boldsymbol{R}_{br} = \boldsymbol{R}_y(\psi_b) \tag{1}$$

As shown in Fig. 2, the wings successively rotate about the x_r and z_w axis with the angles of γ_w and ϑ_w to reach the ultimate position. The rotation matrices for the right wing are

$$\boldsymbol{R}_{rwR} = \boldsymbol{R}_z(\vartheta_{wR})\boldsymbol{R}_x(\gamma_{wR}) \tag{2}$$

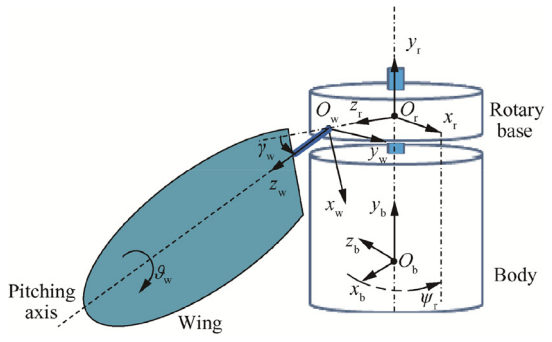

Fig. 2 Reference frames definition of FRW.

The rotation matrices for the left wing, with respect to the rotary base, are combined in the same manner as in Eq. (2). The only difference that the signs of γ_w and ϑ_w are interchanged for the right and left wings.

Combining Eqs. (1) and (2), the rotation matrices from the body frame to right and left wing-fixed frames are

$$\boldsymbol{R}_{\mathrm{bwR}} = \boldsymbol{R}_{\mathrm{rwR}}\boldsymbol{R}_{\mathrm{br}}, \boldsymbol{R}_{\mathrm{bwL}} = \boldsymbol{R}_{\mathrm{rwL}}\boldsymbol{R}_{\mathrm{br}} \tag{3}$$

3. Dynamic model of FRW

3.1. Method and assumption

The flapping wing vehicle is modeled as a system of three rigid bodies: a central body of rotary base with two rigid wings attached at ideal hinges. The method chosen to derive the equations of motion is D'Alembert's Principle Extended to Multiple Rigid Bodies.[15] The functions of generalized inertia force are described as

$$Q_j^* = \sum_{i=1}^{3}(\boldsymbol{F}_i^*\boldsymbol{\gamma}_{ij} + \boldsymbol{M}_i^*\boldsymbol{\beta}_{ij}) \tag{4}$$

where i presents the number of rigid bodies and j denotes the number of generalized coordinates. $\boldsymbol{\gamma}_{ij}$ represents velocity coefficients. $\boldsymbol{\beta}_{ij}$ are angular velocity coefficients. The inertia force $\boldsymbol{F}_i^*$ and moment $\boldsymbol{M}_i^*$ of the ith rigid body are given as

$$\begin{aligned} \boldsymbol{F}_i^* &= m_i(\dot{\boldsymbol{v}}_i + \ddot{\boldsymbol{\rho}}_i) \\ \boldsymbol{M}_i^* &= \boldsymbol{I}_i\dot{\boldsymbol{\omega}}_i + \boldsymbol{\omega}_i \times \boldsymbol{I}_i\boldsymbol{\omega}_i + m_i\boldsymbol{\rho}_i \times \dot{\boldsymbol{v}}_i \end{aligned} \tag{5}$$

where m_i, $\boldsymbol{v}_i$, $\boldsymbol{\rho}_i$, $\boldsymbol{\omega}_i$ and $\boldsymbol{I}_i$ denote the mass, velocities, reference vectors, angular velocities and the resulting mass moments of inertia matrices of the ith rigid body.

In this study, the two wings are assumed to be attached to the rotary base body by joints that allow two degrees of freedom respectively with a common rotation degree of freedom. To simplify the derivation, firstly, the inertia tensors for the individual bodies are calculated with respect to the reference point and they do not need to be calculated at the time-varying center of mass of the system. Then, the body of FRW is assumed to be always fixed on the ground, thereby its motions relative to inertial space are neglected and the body frame is equal to inertial frame. As a result, a dynamic system of three rigid bodies: one for the rotary base, the other two for each wing, are considered. The five degrees of freedom are selected to be described by the generalized coordinates $\boldsymbol{x}_i$, listed together as

$$\boldsymbol{x}_i = [\,\psi_{\mathrm{r}} \quad \vartheta_{\mathrm{wR}} \quad \gamma_{\mathrm{wR}} \quad \vartheta_{\mathrm{wL}} \quad \gamma_{\mathrm{wL}}\,] \tag{6}$$

The related quasi-velocities of coordinates, expressed in inertia frame, are

$$\boldsymbol{u}_i = [\,\omega_{y,\mathrm{r}} \quad \omega_{z,\mathrm{wR}} \quad \omega_{x,\mathrm{wR}} \quad \omega_{z,\mathrm{wL}} \quad \omega_{x,\mathrm{wL}}\,] \tag{7}$$

The variables ω_x, ω_y and ω_z describe the angular velocity of the each selected center rigid bodies in the body frame. Especially, $\omega_{y,\mathrm{r}}$ denotes the rotation angular velocity of the rotary base with two wings, and the flapping and pitching angular velocities of each wing are expressed as $[\,\omega_{z,\mathrm{wR}} \quad \omega_{x,\mathrm{wR}}\,]$ and $[\,\omega_{z,\mathrm{wL}} \quad \omega_{x,\mathrm{wL}}\,]$, respectively.

3.2. Velocities and reference vectors

The angular velocity vector of the wing related to rotary base and expressed in rotation plane frame can be obtained by the time derivative of the two Euler angles $\dot{\gamma}_w$ and $\dot{\vartheta}_w$, which are assumed to be known as the command input. For right wing, the equation is defined as

$$\boldsymbol{\omega}_{\mathrm{wR,r}}^{\mathrm{r}} = \begin{bmatrix} \dot{\gamma}_{\mathrm{wR}} \\ 0 \\ 0 \end{bmatrix} + \boldsymbol{R}_x(\gamma_{\mathrm{wR}})^{\mathrm{T}} \begin{bmatrix} 0 \\ 0 \\ \dot{\vartheta}_{\mathrm{wR}} \end{bmatrix} \tag{8}$$

Related to body mass center, the joint point owns an angular velocity

$$\boldsymbol{\omega}_1 = \boldsymbol{\omega}_{\mathrm{r,b}}^{\mathrm{b}} = [\,0 \quad \dot{\psi}_{\mathrm{r}} \quad 0\,]^{\mathrm{T}} \tag{9}$$

With the combination of Eqs. (8) and (9), the angular velocity of the right and left wings with respect to the body frame, and expressed in the body frame, are

$$\boldsymbol{\omega}_2 = \boldsymbol{\omega}_{\mathrm{r,b}}^{\mathrm{b}} + \boldsymbol{R}_{\mathrm{rb}}\boldsymbol{\omega}_{\mathrm{wR,r}}^{\mathrm{r}}, \quad \boldsymbol{\omega}_3 = \boldsymbol{\omega}_{\mathrm{wL,r}}^{\mathrm{r}} + \boldsymbol{R}_{\mathrm{rb}}\boldsymbol{\omega}_{\mathrm{wL,r}}^{\mathrm{r}} \tag{10}$$

The reference vectors denote the position of the center of mass of the ith body with respect to the reference point. For the rotary base, the reference point is chosen to be its respective center of mass, thereby the reference vector ρ_1 equals zero. In each wing-fixed frame, the positon of mass center owns two components along x_w axis and z_w axis directions:

$$\begin{cases} \boldsymbol{c}_{\mathrm{wR}} = [\,c_{x,\mathrm{wR}} \quad 0 \quad c_{z,\mathrm{wR}}\,]^{\mathrm{T}} \\ \boldsymbol{c}_{\mathrm{wL}} = [\,c_{x,\mathrm{wL}} \quad 0 \quad c_{z,\mathrm{wL}}\,]^{\mathrm{T}} \end{cases}$$

The related reference vectors are transformed from the wing-fixed frames according to

$$\begin{cases} \boldsymbol{\rho}_2 = \boldsymbol{R}_{\mathrm{wRb}}\boldsymbol{c}_{\mathrm{wR}} \\ \boldsymbol{\rho}_3 = \boldsymbol{R}_{\mathrm{wLb}}\boldsymbol{c}_{\mathrm{wL}} \end{cases} \tag{11}$$

Since the translational velocity of the rotary base, the reference velocity v_1 equals zero. And for each of the wings, the reference point of translational velocity is its joint point. The vectors from the center of rotary base to wing joint points, are expressed as $\boldsymbol{r}_{\mathrm{wR}}$ and $\boldsymbol{r}_{\mathrm{wL}}$. As shown in Fig. 1, the vectors defined in body frame own two components along y_b axis and z_b axis directions:

$$\boldsymbol{r}_{\mathrm{wR}} = [\,0 \quad r_y \quad -r_z\,]^{\mathrm{T}}, \quad \boldsymbol{r}_{\mathrm{wL}} = [\,0 \quad r_y \quad r_z\,]^{\mathrm{T}}$$

The reference velocity, for each of the wings, is the velocity of the respective wing joint in the inertia frame. The velocities of the wings are

$$\begin{cases} \boldsymbol{v}_2 = \boldsymbol{\omega}_1 \times \boldsymbol{r}_{\mathrm{wR}} \\ \boldsymbol{v}_3 = \boldsymbol{\omega}_1 \times \boldsymbol{r}_{\mathrm{wL}} \end{cases} \tag{12}$$

The acceleration can be derived by differentiating the above equation

$$\begin{cases} \dot{\boldsymbol{v}}_2 = \dot{\boldsymbol{\omega}}_1 \times \boldsymbol{r}_{\mathrm{wR}} + \boldsymbol{\omega}_1 \times (\boldsymbol{\omega}_1 \times \boldsymbol{r}_{\mathrm{wR}}) \\ \dot{\boldsymbol{v}}_3 = \dot{\boldsymbol{\omega}}_1 \times \boldsymbol{r}_{\mathrm{wL}} + \boldsymbol{\omega}_1 \times (\boldsymbol{\omega}_1 \times \boldsymbol{r}_{\mathrm{wL}}) \end{cases} \tag{13}$$

3.3. Coefficients

The angular velocity coefficients $\boldsymbol{\beta}_{ij}$ are necessary for the derivation of dynamic model, which arise from the calculation

of virtual work performed by moments. Each coefficient is vector and is determined for each rigid body and velocity combination. The angular velocity coefficients are defined as

$$\boldsymbol{\beta}_{ij} = \frac{\partial \boldsymbol{\omega}_i}{\partial \boldsymbol{u}_j}$$

The coefficients of center body of FWR are

$$\boldsymbol{\beta}_{1j} = [\,\boldsymbol{e}_{y,\mathrm{b}} \quad \mathbf{0}_{3\times1} \quad \mathbf{0}_{3\times1} \quad \mathbf{0}_{3\times1} \quad \mathbf{0}_{3\times1}\,] \tag{14}$$

The angular coefficients of right and left wings are

$$\begin{cases} \boldsymbol{\beta}_{2j} = [\,\boldsymbol{R}_{\mathrm{Ib}}^{\mathrm{T}}\boldsymbol{e}_{y,\mathrm{b}} \quad \boldsymbol{R}_{\mathrm{Ib}}^{\mathrm{T}}\boldsymbol{e}_{x,\mathrm{b}} \quad \boldsymbol{R}_{\mathrm{Ib}}^{\mathrm{T}}\boldsymbol{e}_{z,\mathrm{b}} \quad \mathbf{0}_{3\times1} \quad \mathbf{0}_{3\times1}\,] \\ \boldsymbol{\beta}_{3j} = [\,\boldsymbol{R}_{\mathrm{Ib}}^{\mathrm{T}}\boldsymbol{e}_{y,\mathrm{b}} \quad \mathbf{0}_{3\times1} \quad \mathbf{0}_{3\times1} \quad \boldsymbol{R}_{\mathrm{Ib}}^{\mathrm{T}}\boldsymbol{e}_{x,\mathrm{b}} \quad \boldsymbol{R}_{\mathrm{Ib}}^{\mathrm{T}}\boldsymbol{e}_{z,\mathrm{b}}\,] \end{cases} \tag{15}$$

3.4. Mass moments of inertia

For the rotary base, the mass symmetry for xOy and xOz planes is assumed. No planes of mass symmetry are assumed for either wing during the model development. As a result, the resulting mass moments of inertia matrices for each rigid body are

$$\begin{cases} \boldsymbol{I}_1 = \begin{bmatrix} I_{x,\mathrm{b}} & 0 & 0 \\ 0 & I_{y,\mathrm{b}} & 0 \\ 0 & 0 & I_{z,\mathrm{b}} \end{bmatrix} \\ \boldsymbol{I}_2 = \begin{bmatrix} I_{x,\mathrm{wR}} & -I_{xy,\mathrm{wR}} & -I_{xz,\mathrm{wR}} \\ -I_{xy,\mathrm{wR}} & I_{y,\mathrm{wR}} & -I_{yz,\mathrm{wR}} \\ -I_{xz,\mathrm{wR}} & -I_{yz,\mathrm{wR}} & I_{z,\mathrm{wR}} \end{bmatrix} \\ \boldsymbol{I}_3 = \begin{bmatrix} I_{x,\mathrm{wL}} & -I_{xy,\mathrm{wL}} & -I_{xz,\mathrm{wL}} \\ -I_{xy,\mathrm{wL}} & I_{y,\mathrm{wL}} & -I_{yz,\mathrm{wL}} \\ -I_{xz,\mathrm{wL}} & -I_{yz,\mathrm{wL}} & I_{z,\mathrm{wL}} \end{bmatrix} \end{cases} \tag{16}$$

3.5. Motion equations of rotary base

The derived equations of passive rotation motion, with all of the individual pieces together, are presented in vector notation.

$$\begin{aligned} Q_1 = {} & (\boldsymbol{I}_1\dot{\boldsymbol{\omega}}_1 + \boldsymbol{\omega}_1 \times \boldsymbol{I}_1\boldsymbol{\omega}_1)^{\mathrm{T}}\boldsymbol{e}_{y,\mathrm{b}} \\ & + (\boldsymbol{I}_2\dot{\boldsymbol{\omega}}_2 + \boldsymbol{\omega}_2 \times \boldsymbol{I}_2\boldsymbol{\omega}_2 + m_2\boldsymbol{\rho}_2 \times \dot{\bar{\boldsymbol{v}}}_2)^{\mathrm{T}}(\boldsymbol{R}_{\mathrm{br}}^{\mathrm{T}}\boldsymbol{e}_{y,\mathrm{b}}) \\ & + (\boldsymbol{I}_3\dot{\boldsymbol{\omega}}_3 + \boldsymbol{\omega}_3 \times \boldsymbol{I}_3\boldsymbol{\omega}_3 + m_3\boldsymbol{\rho}_3 \times \dot{\bar{\boldsymbol{v}}}_3)^{\mathrm{T}}(\boldsymbol{R}_{\mathrm{br}}^{\mathrm{T}}\boldsymbol{e}_{y,\mathrm{b}}) \end{aligned} \tag{17}$$

The rotations of the right wing and the left wings are described by Eqs. (18) and (19), respectively.

$$\begin{cases} Q_2 = (\boldsymbol{I}_2\dot{\boldsymbol{\omega}}_2 + \boldsymbol{\omega}_2 \times \boldsymbol{I}_2\boldsymbol{\omega}_2 + m_2\boldsymbol{\rho}_2 \times \dot{\boldsymbol{v}}_2)^{\mathrm{T}}(\boldsymbol{R}_{\mathrm{Ib}}^{\mathrm{T}}\boldsymbol{e}_{x,\mathrm{b}}) \\ Q_3 = (\boldsymbol{I}_2\dot{\boldsymbol{\omega}}_2 + \boldsymbol{\omega}_2 \times \boldsymbol{I}_2\boldsymbol{\omega}_2 + m_2\boldsymbol{\rho}_2 \times \dot{\boldsymbol{v}}_2)^{\mathrm{T}}(\boldsymbol{R}_{\mathrm{Ib}}^{\mathrm{T}}\boldsymbol{e}_{z,\mathrm{b}}) \end{cases} \tag{18}$$

$$\begin{cases} Q_4 = (\boldsymbol{I}_3\dot{\boldsymbol{\omega}}_3 + \boldsymbol{\omega}_3 \times \boldsymbol{I}_3\boldsymbol{\omega}_3 + m_3\boldsymbol{\rho}_3 \times \dot{\boldsymbol{v}}_3)^{\mathrm{T}}(\boldsymbol{R}_{\mathrm{Ib}}^{\mathrm{T}}\boldsymbol{e}_{x,\mathrm{b}}) \\ Q_5 = (\boldsymbol{I}_3\dot{\boldsymbol{\omega}}_3 + \boldsymbol{\omega}_3 \times \boldsymbol{I}_3\boldsymbol{\omega}_3 + m_3\boldsymbol{\rho}_3 \times \dot{\boldsymbol{v}}_3)^{\mathrm{T}}(\boldsymbol{R}_{\mathrm{Ib}}^{\mathrm{T}}\boldsymbol{e}_{z,\mathrm{b}}) \end{cases} \tag{19}$$

Here, Q_1 is the rotational moment acted on rotary base. The generalized forces Q_2, Q_3 are the control moment for the right wing, and Q_4, Q_5 are the control moments for the left wing.

The rotation moment, expressed in body frame, can be dived as aerodynamic moments $\boldsymbol{M}_{\mathrm{aero}}$ produced by flapping wings and gravity moments $\boldsymbol{M}_{\mathrm{mass}}$ due to the mass of wings. In this study, the quasi-steady theory is used to calculate the aerodynamic moments $\boldsymbol{M}_{\mathrm{w}}$ produced by flapping wings. The calculation model is given in the following chapter. For each wing, the $\boldsymbol{M}_{\mathrm{mass}}$ is calculated according to

$$\boldsymbol{M}_{\mathrm{massR}} = (\boldsymbol{\rho}_2 + \boldsymbol{r}_{\mathrm{wR}}) \times \left(\boldsymbol{R}_{\mathrm{Ib}} \begin{bmatrix} 0 \\ m_2 g \\ 0 \end{bmatrix} \right) \tag{20}$$

$$\boldsymbol{M}_{\mathrm{massL}} = (\boldsymbol{\rho}_3 + \boldsymbol{r}_{\mathrm{wL}}) \times \left(\boldsymbol{R}_{\mathrm{Ib}} \begin{bmatrix} 0 \\ m_3 g \\ 0 \end{bmatrix} \right) \tag{21}$$

where $\boldsymbol{R}_{\mathrm{Ib}}$ denotes the transfer matrix from inertial frame to body frame. As the assumption of this study, we have $\boldsymbol{R}_{\mathrm{Ib}} = \boldsymbol{I}$. As a result, the $\boldsymbol{M}_{\mathrm{mass}}$ along the y_{b} axis equals zero. That means the gravity of wings will not produce the rotation moment, if the body of FWR does not have angular motion in inertial frame. Then, the rotation moment has an expression as

$$Q_1 = (\boldsymbol{M}_{\mathrm{aeroR}} + \boldsymbol{M}_{\mathrm{aeroL}})\boldsymbol{e}_{y,\mathrm{b}} \tag{22}$$

4. Aerodynamic model

In the numerical study of Wu et al.[7] on FRW, a strong span-wise flow on the wing was observed, and the LEV on the FRW wing merged with the tip vortex and the Trailing Edge Vortex (TEV), forming a vortex ring structure that stayed attached on the wing throughout the flapping cycle. These findings suggest that the quasi-steady model used in this study is applicable for modeling the aerodynamic forces of FRW. As a result, in this study, we extended the quasi-steady aerodynamic model to the application of the flapping and simultaneously rotating wing kinematics of FRW.

Firstly, a geometric model of the FWR wing is chosen and the detailed shape and definition of geometric parameters of the wing are given in Appendix A. For blade element analysis, it is convenient to write down the velocity and acceleration of a 2D wing chord due to the gyration of the wing at span-wise location r. The resultant velocity and acceleration vector when expressed in the wing-fixed frame are planar vectors with only two nontrivial indices, i.e. the x_{w} and y_{w} components:

$$\boldsymbol{v}_{\mathrm{w}}(r) = \boldsymbol{\omega}_{\mathrm{w}} \times \boldsymbol{r} = \omega_{y,\mathrm{w}} r\boldsymbol{e}_{x,\mathrm{w}} - \omega_{x,\mathrm{w}} r\boldsymbol{e}_{y,\mathrm{w}} \tag{23}$$

and

$$\begin{aligned} \dot{\boldsymbol{v}}_{\mathrm{w}}(r) &= (\dot{v}_{x,\mathrm{w}}, \dot{v}_{y,\mathrm{w}}) = \dot{\boldsymbol{\omega}}_{\mathrm{w}} \times \boldsymbol{r} + \boldsymbol{\omega}_{\mathrm{w}} \times (\boldsymbol{\omega}_{\mathrm{w}} \times \boldsymbol{r}) \\ &= (\dot{\omega}_{y,\mathrm{w}} + \omega_{x,\mathrm{w}}\omega_{z,\mathrm{w}}) r\boldsymbol{e}_{x,\mathrm{w}} + (-\dot{\omega}_{x,\mathrm{w}} + \omega_{y,\mathrm{w}}\omega_{z,\mathrm{w}}) r\boldsymbol{e}_{y,\mathrm{w}} \end{aligned} \tag{24}$$

where $\boldsymbol{e}_{x,\mathrm{w}}$, $\boldsymbol{e}_{y,\mathrm{w}}$ and $\boldsymbol{e}_{z,\mathrm{w}}$ denote the unit vectors of right wing frame; $\boldsymbol{\omega}_{\mathrm{w}}$ is the angular velocity vector of the right wing related to inertia frame and expressed in wing frame. For two wings, the related $\boldsymbol{\omega}_{\mathrm{wR}}$ and $\boldsymbol{\omega}_{\mathrm{wL}}$ are obtained as

$$\boldsymbol{\omega}_{\mathrm{wR}} = \boldsymbol{R}_{\mathrm{IwR}}^{-1}\boldsymbol{\omega}_2, \quad \boldsymbol{\omega}_{\mathrm{wL}} = \boldsymbol{R}_{\mathrm{IwL}}^{-1}\boldsymbol{\omega}_3 \tag{25}$$

Since the velocity and acceleration of wing are expressed in wing frame, the effective Angle of Attack (AOA) of the wing α_{e} can be easily found by inverse trigonometric function of the velocity components ratio of the wing:

$$\alpha_{\mathrm{e}} = \arctan\left(\frac{v_{y,\mathrm{w}}}{v_{x,\mathrm{w}}}\right) \tag{26}$$

In quasi-steady theory of flapping wing, this relationship holds, except that the force vector acts perpendicular to the wing chord.[16] The quasi-steady forces are divided by translational forces, rotational forces and virtual mass forces, and the corresponding coefficients are experimentally measured.[17–19] Here, we will use this definition. The corresponding equations for translational force $\boldsymbol{F}_{\mathrm{t}}$ and rotational force $\boldsymbol{F}_{\mathrm{r}}$ for two wings are expressed as

$$\mathrm{d}\boldsymbol{F}_{\mathrm{t}} = (\mathrm{d}F_{x,\mathrm{t}}, \mathrm{d}F_{y,\mathrm{t}}) = \frac{1}{2}\boldsymbol{C}_{\mathrm{t}}\rho\|\boldsymbol{v}(r)\|^2 c(r)\mathrm{d}r \tag{27}$$

And

$$\mathrm{d}F_{\mathrm{r}} = \mathrm{d}F_{y,\mathrm{r}} = -C_{\mathrm{r}}\rho\|\boldsymbol{v}(r)\|\omega_{z,\mathrm{w}}c(r)^2\mathrm{d}r \tag{28}$$

where ρ is the density of the surrounding air. C_{r} is the rotational force coefficient due to wing pitching, and the value of this coefficient is chosen as $C_{\mathrm{r}} = 1.6$ in our calculation. The vector $\boldsymbol{C}_{\mathrm{t}}$ is the translational force coefficient and can be treated as a unit force vector acting on the wing. In the velocity direction, $\boldsymbol{C}_{\mathrm{t}}$ is expressed as life coefficient C_L and drag coefficient C_D, and can be approximated by the following equations[20]:

$$\begin{cases} C_L = C_{L\max}\sin(2\alpha_{\mathrm{e}}) \\ C_D = 0.5(C_{D\max} + C_{D0}) - 0.5(C_{D\max} - C_{D0})\cos(2\alpha_{\mathrm{e}}) \end{cases} \tag{29}$$

where the constant coefficients $C_{L\max}$, $C_{D\max}$ and C_{D0} at the specific Reynolds number ($Re \approx 4000$) are valued from 3D CFD case calculations result. The values are given as: $C_{L\max} = 0.18$, $C_{D\max} = 3.4$, $C_{D0} = 0.05$.

Since we calculate the force and moment in the wing frame, the translational force coefficient $\boldsymbol{C}_{\mathrm{t}}$ can be obtained as

$$\boldsymbol{C}_{\mathrm{t}} = \begin{bmatrix} C_H \\ C_V \end{bmatrix} = \begin{bmatrix} \cos\alpha_{\mathrm{e}} & -\sin\alpha_{\mathrm{e}} \\ \sin\alpha_{\mathrm{e}} & \cos\alpha_{\mathrm{e}} \end{bmatrix} \begin{bmatrix} C_D \\ C_L \end{bmatrix} \tag{30}$$

where C_H is the translational force coefficient along x_{w} axis, and C_V is the translational force coefficient along y_{w} axis.

For the calculation of the aerodynamic torque, the location of the Centre of Pressure (CP) at a chord-wise location r is defined as $\boldsymbol{r}_{\mathrm{CP}} = x_{\mathrm{CP}}\boldsymbol{e}_{x,\mathrm{w}} + r\boldsymbol{e}_{z,\mathrm{w}}$. As a result, the aerodynamic torque of the above two forces can be decided by the following equation:

$$\mathrm{d}\boldsymbol{M}_{\mathrm{q}} = \boldsymbol{r}_{\mathrm{CP}} \times (\mathrm{d}\boldsymbol{F}_{\mathrm{t}} + \mathrm{d}\boldsymbol{F}_{\mathrm{r}}) \tag{31}$$

The virtual mass force and moment are calculated using Sedov's formula,[18] which is suitable for our coordinate definition:

$$\begin{aligned} \mathrm{d}\boldsymbol{F}_{\mathrm{a}} &= (\mathrm{d}F_{x,\mathrm{a}}, \mathrm{d}F_{y,\mathrm{a}}) \\ &= \omega_z(\lambda_{\mathrm{a}}v_y + \lambda_{\mathrm{a}\omega}\omega_z)\boldsymbol{e}_{x,\mathrm{w}}\mathrm{d}r \\ &\quad - (\lambda_{\mathrm{a}}\dot{v}_y + \lambda_{\mathrm{a}\omega}\dot{\omega}_z)\boldsymbol{e}_{y,\mathrm{w}}\mathrm{d}r \\ \mathrm{d}\boldsymbol{M}_{\mathrm{a}} &= \boldsymbol{r}_{\mathrm{CP}} \times \mathrm{d}\boldsymbol{F}_{\mathrm{a}} \end{aligned} \tag{32}$$

where v_y and ω_z can be obtained from the vectors $\boldsymbol{\omega}_{\mathrm{w}}$, $\boldsymbol{v}_{\mathrm{w}}$ of the each wing. λ_{a} and $\lambda_{\mathrm{a}\omega}$ are the added mass force coefficients, which are obtained as

$$\begin{aligned} \lambda_{\mathrm{a}} &= \frac{\pi}{4}\rho c(r)^3 \\ \lambda_{\mathrm{a}\omega} &= \left(\frac{\pi}{4}\hat{h}^2 + \frac{\pi}{128}\right)\rho c(r)^4 \end{aligned} \tag{33}$$

After integrating Eqs. (22), (28), (31) and (32) along the wing span orientation, as a result, the total aerodynamic forces and moments, expressed in body frame, are obtained as

$$\begin{aligned} \boldsymbol{F}_{\mathrm{aero}} &= \boldsymbol{R}_{\mathrm{bw}}^{\mathrm{T}}(\boldsymbol{F}_{\mathrm{t}} + \boldsymbol{F}_{\mathrm{r}} + \boldsymbol{F}_{\mathrm{a}}) \\ \boldsymbol{M}_{\mathrm{aero}} &= \boldsymbol{R}_{\mathrm{bw}}^{\mathrm{T}}(\boldsymbol{M}_q + \boldsymbol{M}_{\mathrm{a}}) \end{aligned} \tag{34}$$

The forces and moments for each wings are calculated based on its velocity and angular velocity respectively. Then, the necessary aerodynamic moments $\boldsymbol{M}_{\mathrm{aeroR}}$ and $\boldsymbol{M}_{\mathrm{aeroL}}$ in Eq. (22) are obtained.

5. Simulation conditions

5.1. Kinematic functions of wings

In this study, we use simple harmonic functions to describe the flapping and pitching motion of the wing, as previous studies for insects flight.[21,22] The kinematic functions of the wing is specified by giving the variation functions:

$$\gamma_{\mathrm{w}} = -\frac{\Delta\gamma_{\mathrm{w}}}{2}\sin(f_{\mathrm{F}}t) \tag{35}$$

$$\vartheta_{\mathrm{w}} = \Delta\alpha\sin\left(f_{\mathrm{F}}t + \frac{\pi}{2}\right) + \alpha_0 \tag{36}$$

where f_{F} is the flapping frequency, $\Delta\gamma_{\mathrm{w}}$ is the flapping amplitude angle, and $\Delta\alpha$ is the pitching amplitude; for modeling the asymmetric pitching, the angle α_0 is introduced. By this definition, the calculation functions between $\Delta\alpha$, α_0 with the geometric AOA of the wing at mid up-stroke angle α_{U} and mid down-stroke angle α_{D} are given as

$$\Delta\alpha = \frac{\alpha_{\mathrm{D}} - \alpha_{\mathrm{U}}}{2},\ \alpha_0 = \frac{\alpha_{\mathrm{D}} + \alpha_{\mathrm{U}}}{2} \tag{37}$$

The time history of flapping motion and pitching motion is plotted as an example in Fig. 3 to illustrate the relationship between flapping motion γ_{w} and pitching motion ϑ_{w} ($\Delta\gamma_{\mathrm{w}} = 30°$, $f_{\mathrm{F}} = 22$ Hz, $\alpha_{\mathrm{U}} = -30°$, $\alpha_{\mathrm{D}} = 20°$).

5.2. Nondimensional coefficients

We used the mean chord length of the wing $\bar{c}$ and the mean flapping velocity at the wingtip $v_{\mathrm{t}} = 2\Delta\gamma_{\mathrm{w}}f_{\mathrm{F}}R$ as the reference length and reference velocity. The aerodynamic lift and rotation moment coefficients are thus defined as

$$C_L = \frac{F_y}{0.5\rho v_{\mathrm{t}}^2 S_{\mathrm{w}}},\ C_R = \frac{-M_{x\_\mathrm{aero}}}{0.5\rho v_{\mathrm{t}}^2 S_{\mathrm{w}}c} \tag{38}$$

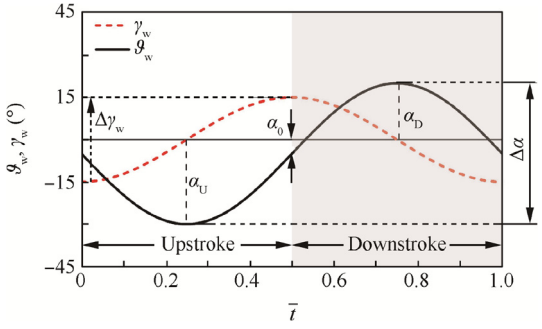

Fig. 3 Kinematic pattern and parameter definition of FRW wing.

Here, F_y and M_{x_aero} mean aerodynamic lift and rotational moment, $\bar{C}_L$ and $\bar{C}_R$ are the averaging aerodynamic lift and rotational moment coefficients during one flapping period, which are obtained by

$$\bar{C}_L = \frac{\int_{t_0}^{t_0+T_F} C_L \mathrm{d}t}{T_F},\ \bar{C}_R = \frac{\int_{t_0}^{t_0+T_F} C_R \mathrm{d}t}{T_F} \tag{39}$$

where t_0 is the initial time at the beginning of one flapping period and T_F means the flapping period. If the effect of geometric shape on aerodynamics is not considered, then the flapping period T_F only depends on frequency f_F.The energetic cost of the FRW's wings can be calculated by the time averaged power efficiency coefficient over a flapping period T_F. For a practical MAV design, elastic storage is desirable for energy efficiency, of which the order is decided by the design property of the mechanical system.

In the current study, we consider that the mechanical system of the FRW can fully store the input power. The instantaneous aerodynamic power efficiency coefficient for hovering flight due to gyration equals directly minus dot product of the angular velocity vector $\boldsymbol{\omega}_w$ with the aerodynamic torque $\boldsymbol{M}_{aero}$:

$$P_f = -\boldsymbol{\omega}_{wR} \cdot \boldsymbol{M}_{aeroR} - \boldsymbol{\omega}_{wL} \cdot \boldsymbol{M}_{aeroL} \tag{40}$$

then, the average power efficiency coefficient is given by

$$\bar{P}_f = \frac{\int_{t_0}^{t_0+T_F} (P_f) \mathrm{d}t}{T_F} \tag{41}$$

A nondimensional variable $\bar{t} = t/T_F$ is defined to describe clearly the time courses of wing motion during a flapping period. As shown in Fig. 3, $\bar{t} \in [0, 0.5]$ indicates that the wing's motion is in the phase of up-stroke, whereas $\bar{t} \in [0.5, 1.0]$ indicates that the wing's motion is in the phase of down-stroke.

5.3. Validation

To validate the compatibility of the aerodynamic model, we compare the calculation results of our model with 3D CFD results presented by Wu et al.,[7] who studied the aerodynamic characteristic of FRW at a low Reynolds Number. In Wu's work,[7] the CFD mode employed a boundary fitted dynamic grid to orientate the wing boundary at a different time with the prescribed kinematics. An OH type mesh was used for flow simulation. Grid 1 has dimensions of $31 \times 33 \times 37$ (in normal, chordwise, and spanwise directions, respectively); and grids 2 and 3 have dimensions of $51 \times 57 \times 61$ and $81 \times 81 \times 91$, respectively. The outer boundary for these grids is located $30c$ away from the wing surface and $15c$ away from the wingtip. The first grid spacings from the wing surface of the three grids are 0.002, 0.001, and 0.0005.

In the benchmark case, the flapping and pitching motions may be defined by the previous descriptions. In the example in CFD results of Wu et al.,[7] the dynamic of rotation motion is ignored and the rotation speed is assumed to be constant, and we use the same model to describe the rotation motion in this case.

$$\psi_j = -\psi_{j0} t \tag{42}$$

where ψ_{j0} is the rotating speed.

Since the kinematics of FWR is combined by steady rotation and reciprocal flapping motion, a nondimensional rotation speed k_R is defined to measure the deflection of the effective AOA:

$$k_R = \frac{\psi_{j0}}{f_F} \tag{43}$$

Based on Eq. (43), ψ_{j0} can be obtained.

The necessary parameters in Eqs. (35), (37) and (43) for validation case are $\Delta\gamma_w = 30°$, $f_F = 22$ Hz, $\alpha_U = -30°$, $\alpha_D = 0°$, $k_R = 0.25$. The Reynolds number for flapping flight may be defined by $Re = v_t \bar{c}/v$, where v is the kinematic viscosity of the air. In this case, we have $Re = 4058$. As shown in Fig. 4, a reasonable agreement is achieved between the lift and rotation moment trends obtained from the present model and CFD results. The averaging coefficients of the present model are $\bar{C}_L = 0.99$ and $\bar{C}_R = 0.173$, while $\bar{C}_L = 0.972$ and $\bar{C}_R = 0.168$ in CFD results. Thereby, the case study shows that the model employed in the present study is credible.

6. Results and analysis

6.1. Analysis of a typical case

A typical case ($\Delta\gamma_w = 30°$, $f_F = 22$ Hz, $\alpha_U = -30°$, $\alpha_D = 20°$, $Re = 4058$) is selected and discussed in this section to investigate the rotation performance of the FRW with the structural parameters listed in Table 1.

The result of the rotation angular velocity varying with time is presented in Fig. 5, and the rotational moment coefficient C_R and its averaging value $\bar{C}_R$ in each flapping periods are given in Fig. 6. It can be clearly seen that the aerodynamic rotational moment in the up-stroke decreases to negative value with the increase of the rotational velocity, and the aerodynamic average rotational moment finally decreases close to zero after fifteen flapping periods, and then maintains at a small value continually. It differs from other existing kinematics with prescribed wing motion, such as rotary wing and insects flapping wing.

However, note that $\bar{C}_R$ of each period cannot converge to zero strictly and ω_{yr} oscillates continuously with an amplitude of ± 0.5 r/s, even after a lot of flapping periods. It is caused by inertia coupling phenomenon of two wings, which are not symmetrical about the axis of rotation. According to Table 1, if the inertial products $I_{xy,w}$, $I_{xz,w}$ and $I_{yz,w}$ are small and ignored, according to Eqs. (17) and (22), the inertia coupling rotation moment M_{coupl} can be expressed as

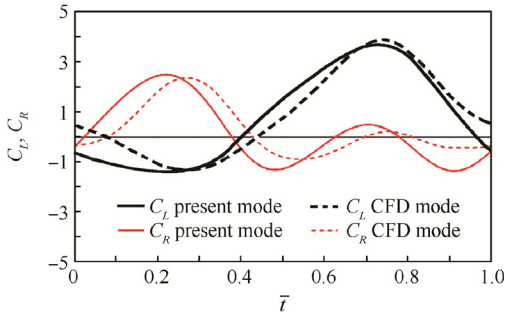

Fig. 4 Comparisons of instantaneous lift and rotational moment coefficients.

Table 1 Basic parameters of FRW.

Parameter		Value
Mass of wing m_2, m_3 (g)		0.15
Mass of rotation body m_1 (g)		0.38
Inertia moment of wing	$I_{x,w}$ (10^{-6} kg·m^2)	2.225
	$I_{y,w}$ (10^{-6} kg·m^2)	1.308
	$I_{z,w}$ (10^{-7} kg·m^2)	9.020
	$I_{xy,w}$ (10^{-7} kg·m^2)	1.128
	$I_{xz,w}$ (10^{-8} kg·m^2)	5.516
	$I_{yz,w}$ (10^{-8} kg·m^2)	1.478
Inertial moment of rotary base $I_{y,b}$ (10^{-8} kg·m^2)		4.8

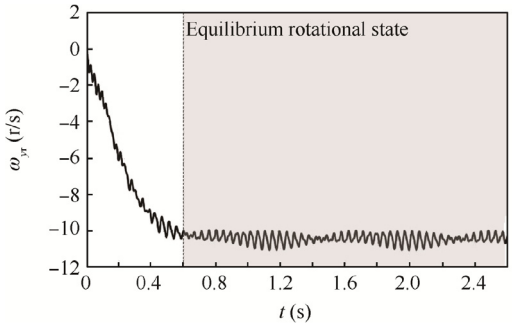

Fig. 5 Rotation angular velocity with varying time.

$$M_{\text{coupl}} = (I_{z,w} - I_{x,w})(\omega_{2x}\omega_{2z} + \omega_{3x}\omega_{3z})$$

Similar to coefficients C_R and $\bar{C}_R$, the coefficients of M_{coupl} are defined as

$$C_{R\text{coupl}} = \frac{-M_{\text{coupl}}}{0.5\rho v_t^2 S_w c}$$

$$\bar{C}_{R\text{coupl}} = \frac{\int_{t_0}^{t_0+T_F} C_{R\text{coupl}}\,\mathrm{d}t}{T_F}$$

Fig. 7 gives the result of rotation coefficients $C_{R\text{coupl}}$ and $\bar{C}_{R\text{coupl}}$ in each flapping period. After the comparison with Fig. 7, it can be seen that the inertia coupling rotation moment always exists even because of the high-speed flapping and pitching motions of two wings. As a result, the rotational moment is balanced with not only the resistance drag of the fluid, but also inertia coupling moment. However, the inertia coupling moment is small compared with the aerodynamic moment, and the total moment is still zero. Consequently, an FWR would reach and stay in an equilibrium rotation speed. In this study, we define the motion status of $\bar{C}_R$ near zero as the Equilibrium Rotational Status (ERS) for FRW.

Fig. 8 gives the results of lift coefficients C_L and $\bar{C}_L$ in each flapping period. As a comparison, constant rotational velocity model with $k_R = 0.47$ is used to calculate the same case. It can be seen from Fig. 8(a) that the lift coefficient vastly increases with the increasing rotational velocity, especially in the upstroke, where the large negative lift becomes positive at the rotational equilibrium state. As a result, as shown in Fig. 8 (b), the variance of $\bar{C}_L$ is increasing gradually and reaches the equilibrium value finally. Only in this time, the lift force of FRW keeps stable with certain kinematic parameters input. Notably, the lift generation of FRW presents first-order inertia system characteristics for a new kinematics of wings input because of the inertia damping in passive rotation motion. That is different from the motions of rotary wing and insect flapping wing, the life force of whom changes and reaches stable immediately with the variance of wings kinematics.[4,13] Thereby, the dynamic inertia time-lag phenomena of lift generation due to passively induced rotational velocity is a unique feature of the FRW configuration.

In order to assess the dynamic system for lift generation, a time-lag constant parameter τ_{aero} is defined to present the time cost of arriving ERS. In this case, the τ_{aero} is obtained as 0.68 s, which equivalent to 15 flapping period.

The following figures present a comparison between the simulation results of $\bar{C}_R$ and $\bar{C}_L$ with the full, 2 times, 4 times and 1/2 times rotational moment of inertia of wings $I_{y,w}$. Fig. 9 shows that as the rotational moment of inertia of the wings relative to the central body increase, the inertia time-lag phenomena of lift generation becomes serious. τ_{aero} changes from 0.41 s, corresponding to 1/2 times $I_{y,w}$, to 2.72 s, corresponding to 4 times $I_{y,w}$. However, once FWR reaches and stays in an

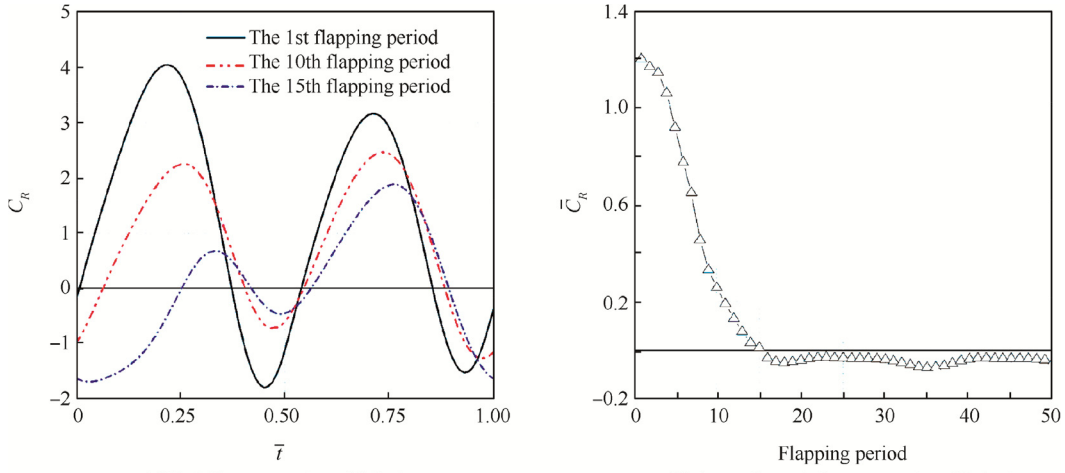

(a) Rotation moment coefficients (b) Averaging rotation moment coefficients

Fig. 6 Rotation moment coefficients C_R varying in the 1st, 10th, 15th flapping period and averaging rotation moment coefficients $\bar{C}_R$ in each flapping period.

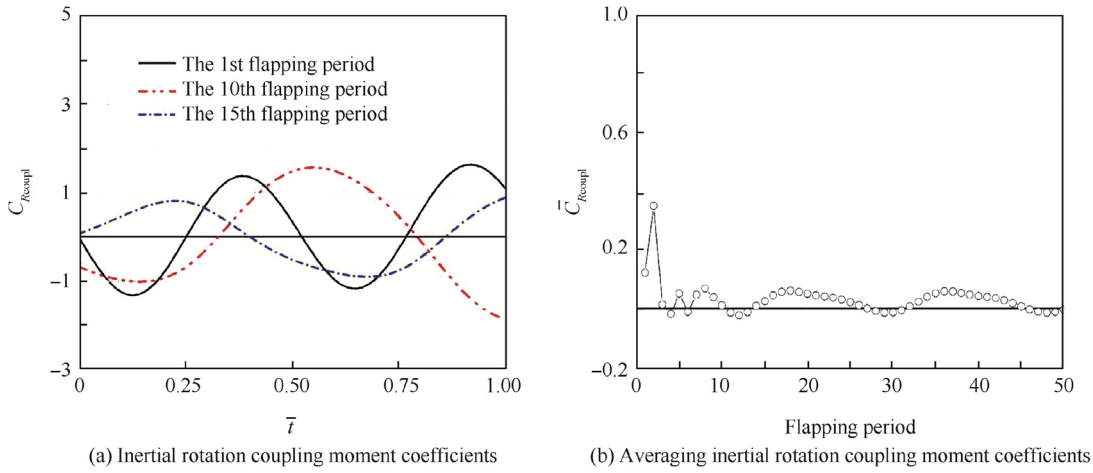

(a) Inertial rotation coupling moment coefficients (b) Averaging inertial rotation coupling moment coefficients

Fig. 7 Inertial rotation coupling moment coefficients $C_{R\text{coupl}}$ varying in the 1st, 10th, 15th flapping period and averaging inertial rotation coupling moment coefficients $\bar{C}_{R\text{coupl}}$ in each flapping period.

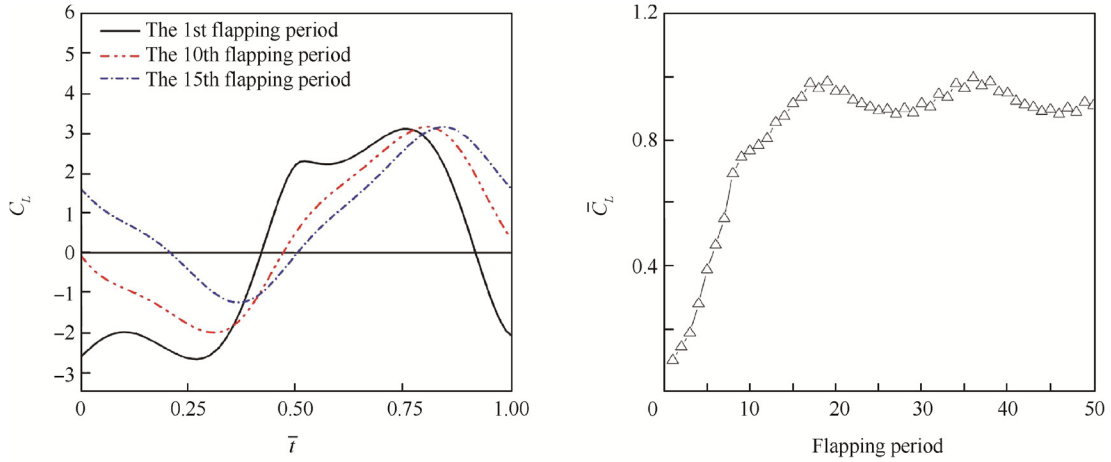

(a) Lift coefficients (b) Averaging lift coefficients

Fig. 8 Lift coefficients C_L varying in the 1st, 10th, 15th flapping period and averaging lift coefficients $\bar{C}_L$ in each flapping period.

equilibrium rotational status, the lift generation is stable and not affected by the variance of $I_{y,\text{w}}$. Thus, a small rotational moment of inertia of wings is useful to decrease time-lag constant.

6.2. Effects of the kinematics of wings

As given in Eq. (36), the pitching kinematics of wings is described as sinusoidal wave functions. For a certain flapping frequency f_F, the pitch angle of the wing at any instantaneous time is decided by AOAs parameters: mid up-stroke α_U and mid down-stroke α_D. The two parameters, donated pitching kinematics, may be selected to analyze the influence of wings kinematics to aerodynamic performance.

In order to present the aerodynamic performance of FRW in the equilibrium rotational status, the period average lift coefficient $\bar{C}_{L\_\text{stab}}$, power efficiency coefficient $\bar{P}_{\text{f}\_\text{stab}}$ and nondimensional rotational velocity $\bar{\mu}_{\text{f}\_\text{stab}}$ are defined as

$$\bar{C}_{L\_\text{stab}} = \frac{\sum_{i=i_\text{stab}}^{i_\text{stab}+j} \bar{C}_L^i}{j}$$

$$\bar{P}_{\text{f}\_\text{stab}} = \left| \frac{\sum_{i=i_\text{stab}}^{i_\text{stab}+j} \bar{P}_\text{f}^i}{j} \right|$$

$$\bar{\mu}_{\text{f}\_\text{stab}} = \frac{\sum_{i=i_\text{stab}}^{i_\text{stab}+j} \omega_{y\text{r}}^i}{j} \cdot \frac{1}{\Delta\gamma_\text{w} f_\text{F}}$$

where i_stab means the flapping period while FRW has been in the ERS, j is the total number of flapping period used to calculate coefficients, and $\bar{P}_{\text{f}\_\text{stab}}$ is defined as positive always. In this case, we let $j = 10$ to acquire accurate description of aerodynamic performance for FRW.

In a typical case of $\Delta\gamma_\text{w} = 30°$, $f_\text{F} = 22$ Hz, $Re = 4058$, Fig. 10 presents the results of coefficients $\bar{C}_{L\_\text{stab}}$, $\bar{P}_{\text{f}\_\text{stab}}$, $\bar{\mu}_{\text{f}\_\text{stab}}$ and τ_aero, while the mid-up stroke α_U varies from 0° to

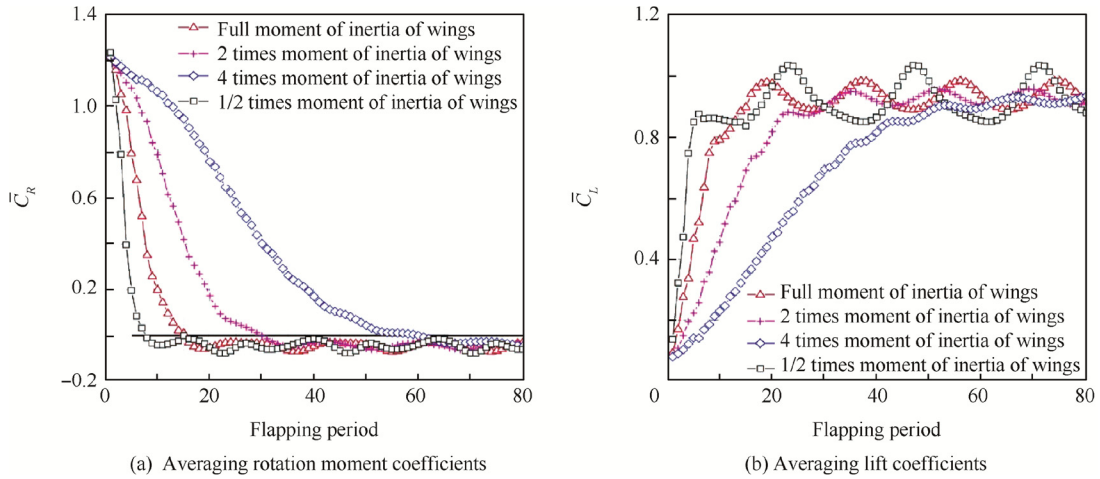

Fig. 9 Averaging rotation moment coefficient $\bar{C}_R$ and averaging lift coefficient $\bar{C}_L$ in each flapping period.

$-90°$ with increments of $-2.5°$, and the mid-down stroke α_D is fixed to $\alpha_D = 10°, 20°, 30°$.

As shown in Fig. 10(a), notice that the lift of FRW is near zero when the α_U equals -α_D, e.g. the lift produced in up-stroke and down-stroke may cancel each other. In order to acquire a high positive lift generation of FRW, we need to increase α_U and decrease α_D. Since in the up-stroke, the high value of α_U makes the wing surface close to the airflow direction decided by rotation motion and flapping motion together. As a result, the negative effective AOA of wing α_e decreases, or even changes to be positive. The negative lift generated in up-stroke phase decreases consequently. On the contrary, the small value of α_D increases the α_e at down-stroke phase, which produces more positive lift force. The power efficiency does not increase with the lift performance improving, while compared with Fig. 10(a) and (b). Since the high drag force follows as high life generation, the optimal lift generation does not correspond to the optimal power efficiency. In addition, a high equilibrium rotation velocity occurs at small AOA parameters while both α_U and α_D are within $20°$ to $-20°$. However, as shown in Fig. 10(c) and (d), high $\bar{\mu}_{f\_stab}$ means more time is required to arrive ERS, thereby the τ_{aero} becomes large for a small α_U and α_D.

In order to present the effect of pitching kinematic on FRW, three zones are defined, which include high lift force zone ($\bar{C}_{L\_stab} \geqslant 1.5$), high power efficiency zone

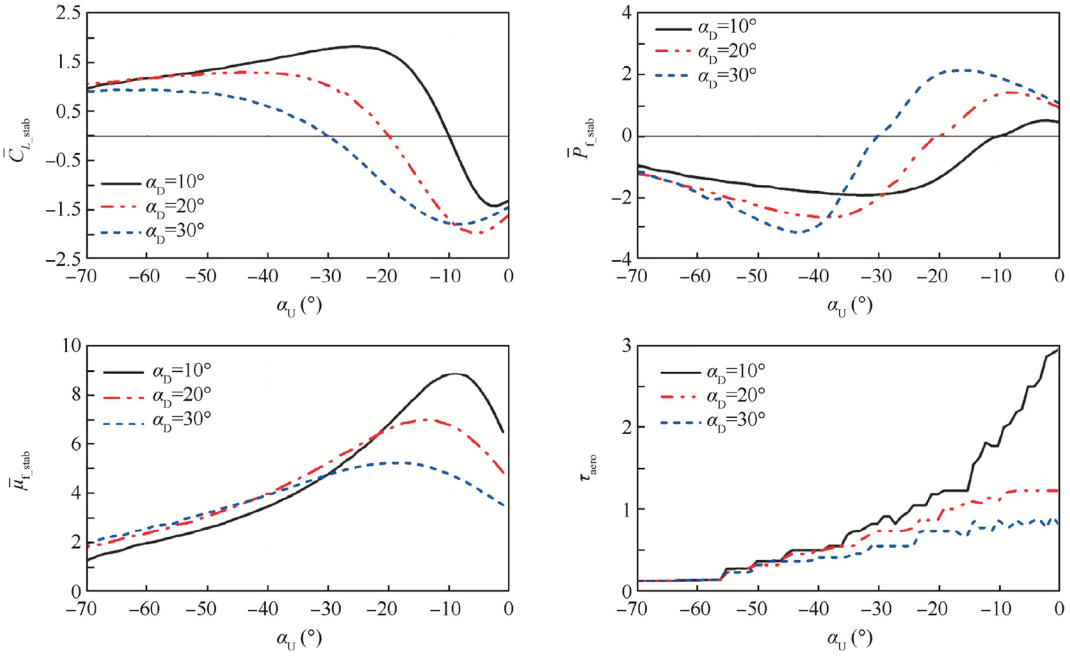

Fig. 10 Period average lift coefficient $\bar{C}_{L\_stab}$, power coefficient $\bar{P}_{f\_stab}$, nondimensional rotational velocity $\bar{\mu}_{f\_stab}$ and time-lag constant parameter τ_{aero} variations with mid-up stroke α_U and mid-down stroke α_D.

Table 2 Maximum nondimensional parameters and the corresponding geometric AOAs.

Parameter	Maximum value	Related parameter				
		α_U (°)	α_D (°)	$\bar{C}_{L\_stab}$	$\bar{P}_{f\_stab}$	τ_{aero}
$\bar{C}_{L\_stab}$	1.975	−20	6		1.51	0.97
$\bar{P}_{f\_stab}$	3.14	−44	30	0.758		0.36

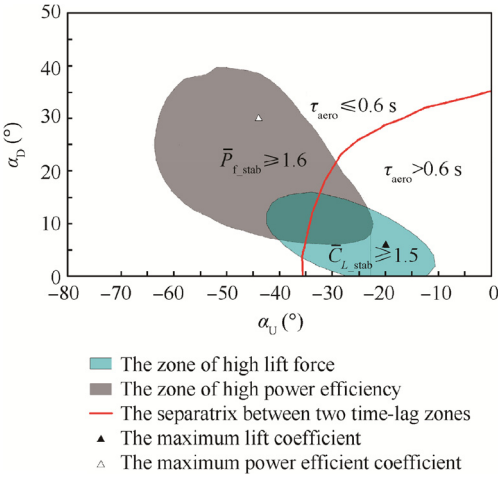

Fig. 11 Zones of high lift, power efficiency and less time-lag distribution variations with mid-up stroke α_U and mid-down stroke α_D.

($\bar{P}_{f\_stab} \geqslant 1.6$) and low time-lag zone ($\tau_{aero} \leqslant 0.6$ s). The maximum nondimensional parameters and the corresponding geometric AOAs are listed in Table 2. Fig. 11 shows three zones distribution as α_U varies from −80° to 0° and α_D varies from 0° to 50°. The maximum lift coefficient $\bar{C}_{L\_stab} = 1.97$ responses the point at $\alpha_U = -20.0°$, $\alpha_D = 6°$, and the maximum power efficiency coefficient happens at $\alpha_U = -53°$, $\alpha_D = 34°$. If taking the high lift, high power efficiency and low time-lag into consideration, as given in Fig. 11, an optimal AOAs parameters occur at the point where α_D is relative small (within 7–15°), and α_U is in the range −35° to −40°.

7. Conclusions

The passive rotation motion and aerodynamic performance of a rotary base with two flapping wings as a simplified model of FRW flight vehicle are studied. The nonlinear, multiple body equations of motion for an FRW is derived using D'Alembert's Principle for Multiple Rigid Bodies. In addition, a quasi-steady aerodynamic model is utilized for the calculation of the aerodynamic forces and moments at a low Reynolds number ($Re \approx 4000$).

The simulation of typical case shows that the passive rotation motion of FRW is a continuous dynamic process of convergence into rotary velocity equilibrium status due to an interaction between aerodynamic thrust and rotation velocity. That causes the unique time-lag of stable lift generation. Even in the rotation equilibrium status, the lift force is still oscillating with small amplitude.

The pitching kinematics of wings greatly affects the equilibrium rotational characteristics, thus the aerodynamic performance of FRW. The lift force generation, power efficiency, equilibrium rotational velocity and dynamic time-lag are studies for various AOA parameters of wings. The result shows that in order to acquire a high positive lift generation with high power efficiency and small dynamic time-lag, a relative high mid up-stroke α_U and low mid down-stroke α_D are necessary. In the zone where α_D is within 7–15° and α_U is within −35° to −40°, the performance of FRW is optimal.

Appendix A.

The geometry of the FRW wing is modeled by keeping the morphological parameters of quasi-static analysis similar with available insects' data. In generation, we assume that the thickness of the wing is small enough and has little effect on the wing's aerodynamic. Thereby, a 2D wing with a span length R is shown in Fig. A1. Along the span direction, the wing is dived by infinite small strip with width dr. The chord length $c(r)$ is shown at a chord-wise location r; h refers to the coordinate of the major axis of the ellipse in x_w axis. The Center of Gravity (CG) of wing has two components x_{CG}, z_{CG} in the wing frame. The AR is within 3–5; the shape parameters, including wing aspect ratio AR, the first, second and third radii of nondimensional moment of wing area ($\hat{r}_1(s)$, $\hat{r}_2(s)$ and $\hat{r}_3(s)$) are: AR = 3.6, $\hat{r}_1(s) = 0.55$, $\hat{r}_2(s) = 0.59$, $\hat{r}_3(s) = 0.63$.

The chord-wise location of Centre of Pressure (CP) is in the x_w axis. Referring to Dickinson et al.,[17] the x_{CP} with respect to location r varies linearly with the change of the effective AOA α_e (given in Eq. (26) and the linear relation can be expressed as

$$x_{CP}(r) = \left(\hat{h} + \frac{0.82}{\pi}|\alpha_e(r)| - 0.45\right)c(r)$$

where $\hat{h}$ is the nondimensional local coordinate of the chord: $\hat{h} = h/c(r)$.

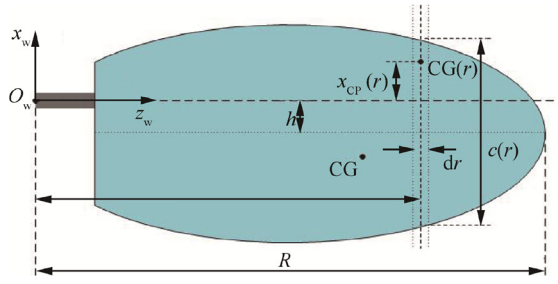

Fig. A1 Geometric parameters definition of FWR wing.

References

1. Pines DJ, Bohorquez F. Challenges facing future micro-air-vehicle development. *J Aircr* 2006;**43**(2):290–305.
2. Vandenberghe N, Zhang J, Childress S. Symmetry breaking leads to forward flapping flight. *J Fluid Mech* 2004;**506**:147–55.
3. Guo S, Yang D, Huang Z. A smart material aeroelastic flapping wing micro rotorcraft. *Int Forum Aeroelasticity Struct Dynam*; 2009.
4. Guo S, Li D, Wu J. Theoretical and experimental study of a piezoelectric flapping wing rotor for micro aerial vehicle. *Aerosp Sci Technol* 2012;**23**(1):429–38.
5. Van Holten T, Heiligers M, Kuiper R. Forced flapping mechanism designs for the Ornicopter: a single rotor helicopter without reaction torque. In: *European rotorcraft forum*; 2004.
6. Zhou C, Wu J, Guo S. Experimental study on the lift generated by a flapping rotary wing applied in a micro air vehicle. *Proc Inst Mech Eng Part G – J Aerospace Eng* 2014;**228**(11):2083–93.
7. Wu J, Wang D, Zhang Y. Aerodynamic analysis of a flapping rotary wing at a low Reynolds number. *AIAA J* 2015;**53**(10):1–16.
8. Li H. Aerodynamic analysis and experiment of a micro flapping wing rotor [dissertation]. Bedford: Cranfield University; 2015.
9. Etkin B, Reid L. *Dynamics of flight: stability and control*. New York: John Wiley & Sons Inc; 1996.
10. Khan Z, Agrawal S. Modeling and simulation of flapping wing micro air vehicles. In: *Proceedings of IDETC/CIE'2005 2005 ASME international design engineering technical conferences; 2005 September 24–28; Long Beach, CA, USA*. New York: ASME; 2005.
11. Gebert G, Gallmeier P, Evers J. Equations of motion for flapping flight. In: *Proceedings of the AIAA atmospheric flight mechanics conference*. Reston: AIAA; 2002.
12. Sun M, Wang J, Xiong Y. Dynamic flight stability of hovering insects. Acta Mech Sin 2007;**23**(3):231–46 [Chinese].
13. Orlowski CT, Girard AR. Modeling and simulation of nonlinear dynamics of flapping wing micro air vehicles. *AIAA J* 2011;**49**(5):969–81.
14. Mahjoubi H, Byl K. Dynamics of insect-inspired flapping-wing MAVs: multibody modeling and flight control simulations. In: *Proceedings of 2014 American control conference (ACC)*; 2014 June 4–6; Portland, Oregon, USA. 2014.
15. Greenwood DT. *Advanced dynamics*. New York: Cambridge University Press; 2006.
16. Usherwood JR, Ellington CP. The aerodynamics of revolving wings I. Model hawkmoth wings. *J Exp Biol* 2002;**205**(11):1547–64.
17. Dickinson MH, Lehmann FO, Sane SP. Wing rotation and the aerodynamic basis of insect flight. *Science* 1999;**284**(5422):1954–60.
18. Wang ZJ, Birch JM, Dickinson MH. Unsteady forces and flows in low Reynolds number hovering flight: two-dimensional computations vs robotic wing experiments. *J Exp Biol* 2004;**207**(3):449–60.
19. Sane SP, Dickinson MH. The control of flight force by a flapping wing: lift and drag production. *J Exp Biol* 2001;**204**(15):2607–26.
20. Whitney JP, Wood RJ. Aeromechanics of passive rotation in flapping flight. *J Fluid Mech* 2010;**660**(1):197–220.
21. Wu JH, Sun M. Unsteady aerodynamic forces of a flapping wing. *J Exp Biol* 2004;**207**(7):1137–50.
22. Bin Abas MF, Bin Mohd Rafie AS, Bin Yusoff H, Bin Ahmad KA. Flapping wing micro-aerial-vehicle: kinematics, membranes, and flapping mechanisms of ornithopter and insect flight. *Chin J Aeronaut* 2016;**29**(5):1159–77.

2018-03-13

Nonlinear dynamics of a flapping rotary wing: Modeling and optimal wing kinematic analysis

Wen, Qiuqiu

Elsevier

Qiuqiu Wen, Shijun Guo, Hao Li and Wei Dong. Nonlinear dynamics of a flapping rotary wing: Modeling and optimal wing kinematic analysis. Chinese Journal of Aeronautics, Volume 31, Issue 5, May 2018, Pages 1041-1052

https://doi.org/10.1016/j.cja.2018.03.004